CRYSTAL GROWTH & DESIGN

Article

pubs.acs.org/crystal

Oriented Calcite Micropillars and Prisms Formed through Aggregation and Recrystallization of Poly(Acrylic Acid) Stabilized Nanoparticles

Xia Long,[†] Yurong Ma,*[,†] Kang Rae Cho,[‡] Dongsheng Li,[‡] James J. De Yoreo,*[,‡] and Limin Qi*[,†]

[†]Beijing National laboratory for Molecular Sciences (BNLMS), State Key Laboratory for Structural Chemistry of Unstable and Stable Species, College of Chemistry, Peking University, Beijing 100871, P.R. China

[‡]Molecular Foundry, Lawrence Berkeley National Laboratory, Berkeley, California 94720, United States

Supporting Information

ABSTRACT: Though calcium carbonate crystals with various morphologies have been successfully fabricated via bioinspired methods, the mechanism underlying crystallization of one-dimensional (1D) calcite microstructures along defined crystallographic axes is poorly understood. In this paper, we first show that by combining the effects of poly(acrylic acid) (PAA) and calcite substrates we can direct the formation of calcite through an intermediate complex of PAA and Ca^{2+} into oriented calcite micropillars with {104} faceted coaligned platelike subunits. Moreover, in situ AFM studies under different conditions than those used in bulk experiments also lead to formation of 1D calcite microstructures. With a slight change in conditions, arrays of oriented calcite prisms with triangular cross sections are formed on calcite substrates. Though distinct in morphology, these pillars and prisms form in a similar way via anisotropic nanoparticle aggregation, growth, fusion, and reorganization. The results may provide new insights into mechanisms of biomineralization.

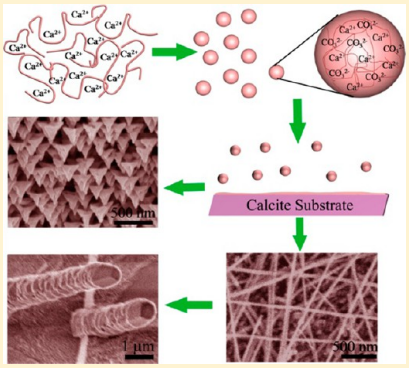

1. INTRODUCTION

Biomimetic synthesis and shape control of calcium carbonate have received much attention owing to its abundance in natural biominerals having remarkable mechanical and optical properties.[1−6] Examples include the spicules of brittle stars,[5] sea urchin spines,[7] the prismatic layer of mollusk shells,[8,9] sea urchin teeth,[10] and coccoliths.[11] Numerous studies have shown that many biogenic minerals form from amorphous precursors,[2,12,13] which are believed to be temporarily stabilized by biomolecules[12,14] or simple inorganic ions such as magnesium ions[15] and silicates.[16] Similar pathways have been obtained in synthetic systems through the use of additives[17−22] or at constant pH values.[23] Gower et al. proposed that the initial phase was, in fact, in a liquidlike state referred to as a polymer-induced liquid precursor (PILP)[17−19] and described the formation of calcium carbonate with nonequilibrium morphologies retained during the PILP-to-crystal transformation process in the presence of polymers.

Calcite mesocrystals with three-dimensional (3D) hierarchical microstructures and internal porosities have also attracted increasing attention due to their mesoscopic structure, single crystal characteristics, and superior mechanical properties, similar to those of minerals found in organisms.[17] The mesocrystal model is based on controlled aggregation of nanoparticles, a process that is similar to what have also been proposed to describe nonclassical crystallization processes,[2,24,25] including formation of intermediary clusters or phase separation to liquid precursors as the primary building blocks, crystallization via amorphous intermediates that can undergo mesoscopic transformations, and oriented attachment of nanoparticulate building blocks with possible subsequent crystallographic fusion of high-energy crystal faces.[26,27] Inspired by nature, in recent years researchers have exploited these nonclassical crystallization mechanisms[6] to form calcite with controlled morphology "on the bench" through the use of organic molecules[28−30] and templates.[31,32] As in biogenic mineralization processes, additives may be occluded into the minerals during biomimetic crystallization processes and thus improve the mechanical properties of the final crystals.[33−36]

Among the variety of morphologies achieved during synthesis of calcium carbonate using the above-mentioned methods, quasi-one-dimensional (1D) calcium carbonate has received a lot of attention and has been successfully synthesized by many research groups through the use of hard templates,[13,37] calcite substrates,[38,39] polyacid block copolymers,[40−44] positively charged additives[45] and microemulsions.[46,47] Ward et al. synthesized 1D calcite at the millimeter scale by using hierarchical self-assembly of 1D metal−organic protein frameworks as templates.[48] Gower's group was the first to grow calcite fibers in an aqueous-based system through the PILP process, using a higher molecular weight of polyaspartic

Received: February 27, 2013
Published: July 31, 2013

acid than is typically used for 3D structures. Fibers appeared to emanate from some large gelatinous globules.[40] In a follow-up paper, using calcite substrates and poly(acrylic acid) additives, Gower's group synthesized high-aspect-ratio single crystalline calcite nanofibers with remnant "bobbles" at the tips of some fibers. They hypothesized that growth occurred through a solution−liquid−solid (SLS) mechanism.[41] Recently, they modified this hypothesis to autocatalytic assembly of nanodroplets/nanoparticles at high energy surface protrusions as a means for generating the 1D growth of fibers in $BaCO_3/SrCO_3$ systems.[49] Kim and coauthors fabricated single crystalline calcite fibers on calcite and aragonite substrates through directional self-assembly of amorphous calcium carbonate precursor units stabilized by a esterificated polyacid diblock copolymer of poly[(ethylene oxide)-block-(glycerol monomethacrylate)] (PEO_{45}-2SA:$PGMA_{48}$).[39] Recently, it was reported that besides acidic macromolecules, positively charged poly(allylamine hydrochloride) could also induce the formation of calcite thin films and fibers.[45]

Even though a number of research groups have successfully synthesized quasi-1D calcite single crystals, the crystallographic direction of the long axis of the fibers was not identified except in the study of Liu and Yates who obtained rodlike calcite with the long axis parallel to the crystallographic *c* axis.[47] More importantly, there is no literature related to controlled crystallization of 1D calcite microstructures along defined crystalline axes that provides an understanding of the formation mechanism. The purpose of this paper is to provide that understanding by investigating the formation of such structures using optical microscopy, FT-IR spectroscopy, SEM and TEM imaging, and in situ atomic force microscopy (AFM). The latter provides information on the dynamics of nucleation, assembly, and growth at the molecular to nanometers scale.[50−52] We first show that by combining the effects of PAA additives, which have many carboxylic groups and can temporarily stabilize amorphous or liquidlike precursors,[41] and calcite substrates, which may control crystal orientation of the crystallizing particles, we can direct the formation of calcite through an intermediate complex of PAA and Ca^{2+} into micropillars composed of platelike subunits that are parallel to the {104} planes of calcite. Gower's group has obtained similar calcite microfibers with stacks of isoriented microfacets.[53] We then demonstrate that by decreasing the concentrations of the Ca precursors and polymer in the mother solutions, arrays of oriented polyhedral prisms can be obtained on calcite substrates. Finally, in situ AFM reveals that calcite micropillars and prisms, though distinct in morphology, form in a similar way via assembly, reorganization, and expansion of nanoparticles into a crystalline microstructure whose orientation is directed by the underling calcite substrate. The roughly spherical shape and consistent size of the nanoparticles implies that they are either ACC or PILP particles, while the regular anisotropic shape of the microstructures shows that their attachment rates and dynamics of reorganization are biased by the anisotropic interactions of these nanoparticles. Therefore, this research reveals the formation mechanism of 1D calcite mesocrystals and thus provides additional guidelines for developing biomimetic materials.

2. EXPERIMENTAL SECTION

Materials: Shells of the bivalve *Atrina rigida* from the east coast of Florida were purchased from Gulf Specimen Marine Laboratories (Panacea, FL). Geological calcite crystals were purchased from Ward's Natural Science. Sea urchin was obtained from the shore of the Yellow Sea, China. 5100 Molecular weight poly(acrylic acid) sodium salts (PAA) were purchased from Sigma-Aldrich. Calcium chloride and ammonium bicarbonate were purchased from Alfa. Calcite (104) substrates were obtained by cleaving platelike calcite rhombohedra from geological calcite single crystals. Calcite (001) substrates were fabricated via two steps. First, calcite crystals with their (001) direction perpendicular to the horizontal plane were embedded into resin. Second, the embedded calcite crystals were ground by SiC abrasive paper and then polished with 0.05 μm Al_2O_3 aqueous suspension until the surfaces became smooth. Substrates formed from fractures of sea urchin tests (SUT) and prisms of mollusk shells of bivalve *A. rigida* were ground by SiC abrasive paper and then polished with 0.05 μm Al_2O_3 suspension until the surfaces were smooth. All of the fabricated substrates were thoroughly washed with water under ultrasonication multiple times to make sure no artifacts remained on the substrate. These substrates were then dried and kept in a desiccator until use. Figure S1 of the Supporting Information reveals that all of these substrates are flat and smooth after polishing.

Fabrication of calcite micropillars by gas diffusion method: 5 mL of aqueous solution with 50 mM $CaCl_2$ and 0.025 mg/mL PAA (MW = 5100) was put in a small beaker. A number of calcite substrates were placed at the bottom of the beaker. The aqueous solution was sealed by aluminum foil with a hole punctured by a syringe needle. Three grams of NH_4HCO_3 powder was placed in a 1 mL weighing bottle and also sealed by aluminum foil containing one hole. Both the aqueous solution and NH_4HCO_3 powder were placed in a sealed desiccator. The crystallization of calcium carbonate was allowed to proceed for 4 days at room temperature (~27 °C), if not noted otherwise. Afterward, the calcite substrates were taken out of the aqueous solutions, washed by distilled water multiple times, and kept in a desiccator prior to characterizations.

Fabrication of nanofibers and prism arrays by the mixing method: a mixing method was employed to fabricate nanofibers in order to study this process by AFM. First, because nanofibers were found to form in solutions produced through the gas diffusion method described above, when the pH was around 9 (see Figure S2 of the Supporting Information), the pH values of both calcium chloride and sodium (bi)carbonate solutions were adjusted to 9 by the addition of sodium hydroxide before mixing. One milliliter of aqueous solution (pH = 9) containing 15 mM of $CaCl_2$ and 0.025 mg/mL of PAA was mixed with 1 mL of aqueous solution containing 15 mM of sodium carbonate/sodium hydrogen carbonate buffer (pH = 9). Calcite (104) substrates were placed at the bottom of the reactor and all of them were rinsed with distilled water and dried with N_2 after the reaction and then characterized by scanning electron microscopy (SEM) and AFM. To obtain an oriented prism array, 10 mM carbonate buffer, 10 mM calcium chloride solution, and 0.01 mg/mL PAA were used instead.

Ex situ and in situ AFM characterization: both ex situ (in air) and in situ (in solution) imaging were done in tapping mode at room temperature with a NanoScope III (Veeco). Silicon and silicon nitride tips were used for ex situ and in situ AFM imaging experiments, respectively. For in situ AFM, a solution containing 15 mM of calcium chloride and 0.025 mg/mL of PAA was mixed with carbonate buffer (pH = 9) and then pumped into a fluid cell where the calcite (104) substrate was placed by PUMP 33 (Harvard Apparatus), at a pumping rate of 5 μL/min. Images were captured continuously.

Other characterizations: the overgrown calcite substrates after reaction were washed with alcohol, dried under room temperature, and characterized by scanning electron microscopy (SEM, Hitachi FE-S4800) at an accelerating voltage of 2.0 kV. Micropillars were gently collected from calcite substrates with a doctor blade, dispersed in alcohol under sonication, and then transferred to copper grid or glass slide for characterization of transmission electron microscopy (TEM, JEM-200CX) at 160 kV or polarized light microscopy (Olympus BX51TRF optical microscopy). Fourier transform-infrared (FT-IR) spectra of collected micropillars were recorded on JEOL and Bruker VECTOR22. A pH curve was produced from measurements performed using a pH meter with the hydrogen ion electrode immersed in a mixed solution of calcium chloride and PAA, which was

placed in a sealed reactor in the presence of a container of NH_4HCO_3 powders. Both solution and NH_4HCO_3 powder were sealed by parafilm, which was pierced with 20 holes by a needle to allow gas diffusion. The pH values at different reaction times were recorded on the pH meter.

3. RESULTS AND DISCUSSION

3.1. Characterizations of Calcite Micropillars. *3.1.1. Calcite Micropillars Formed on Calcite (104) Substrates.* Micropillars with diameters from 250 nm to 1 μm and heights from 1 to more than 10 μm could be observed on the surface of calcite (104) substrates after crystallization for 4 days (Figure 1, panels a–c). All the micropillars were birefringent, as evidenced by the polarized optical microscope (POM) images (Figure S3 of the Supporting Information), indicating a high degree of crystallization. Three smooth rhombohedral planes on the top (Figure 1, panels b and c) and laminated microstructures composed of what appear to be platelike subunits (Figure 1, panels c–e) were revealed by SEM. No helical pattern of growth steps was found; this is in contrast to observations from stacked calcite structures fabricated in microemulsions thought to be formed by helical propagation of surface steps from primary single crystals.[46] In addition to micropillars, macrosteps can be seen on the underlying substrate, which was previously smooth at the resolution of the SEM images.

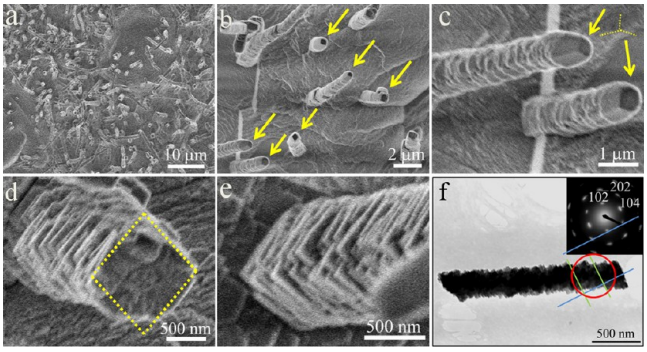

Figure 1. (a–e) SEM images, (f) TEM image, and (f inset) SAED pattern of micropillars formed on a calcite (104) substrate in the presence of PAA. The arrows in (b) and (c) indicate the tops of the micropillars. The concentration of calcium chloride and PAA were 50 mM and 0.025 mg/mL, respectively. The reaction time was 4 days. Red circle in (f) indicates the area selected for collection of the SAED pattern.

FT-IR was employed to determine the chemical composition of micropillars (Figure S4 of the Supporting Information). The ν_3, ν_2, and ν_4 vibration bands of carbonate groups of calcite appeared at 1425, 875, and 712 cm^{-1}, respectively, indicating that micropillars were composed of calcite. The selected area electron diffraction (SAED) pattern (Figure 1f inset) was obtained from part of a single micropillar. The slight elongation of the electron diffraction spots indicates that the pillars are single crystals with slight mosaicity, rather than a composite of a few separate single crystals or a polycrystalline structure.[2,24,25]

TEM images (Figure 1f and Figure S5 of the Supporting Information) show that the apparent subunit boundaries that give rise to the platelike morphology (parallel to the green lines in Figure S5 of the Supporting Information and Figure 1f) do not penetrate the bulk of the pillars. The top and bottom facets of these plates were almost parallel to the {104} face of the calcite substrate, exhibiting only a few degrees of misorientation. However, the long axis of the micropillars is not precisely perpendicular to the {104} plane of the calcite substrate, typically being 0 to 30 degrees off.

3.1.2. Calcite Micropillars Formed on Other Substrates. Similar experiments have been performed on other calcite substrates, including polished geogenic calcite crystals exposing the (001) plane [calcite (001)], polished sea urchin tests (SUT), and prismatic layers of mollusk shells (prisms). It is noteworthy that both of the polished surfaces of SUT and mollusk shell prisms are calcite (001) planes, with the same crystallographic orientation as the geogenic calcite (001) substrates. The SEM images shown in Figure S6 of the Supporting Information revealed that calcite micropillars formed and covered most of the surfaces of calcite (001), polished sea urchin tests (SUT), and prisms of mollusk shells but were arranged in a more disordered way than those grown on calcite (104) substrates (Figure 1). From zoomed in SEM images shown in Figure 2, one can see that calcite micropillars grown on biogenic calcite substrates (SUT or prisms) had slightly larger diameters (>300 nm) than those formed on geogenic calcite (001) substrates (~250 nm). More interestingly, in addition to micropillars, a layer of rhombohedral calcite crystals with the same orientation as calcite (001) substrates could also be observed in zoomed-in SEM images (Figure 2, insets of panels b and c). These were formed through epitaxial growth and were similar to those formed on the same substrates without any additive (Figure S7, panels a and b, of the Supporting Information). Indeed, as was observed for micropillars formed on calcite (104) substrates, TEM images and corresponding SAED patterns indicated that the micropillars formed on calcite (001), SUT, and prismatic layers were also calcite with the apparent morphology of mesocrystals composed of platelike subunits parallel to the {104} planes of calcite. Similar microfacets iso-oriented with the long axis of the figures have been observed in Gower's work.[41] Similar procedures were carried out on silicon (Figure S8, panels a and b, of the Supporting Information) and glass substrates (Figure S8, panels c and d, of the Supporting Information). However, only spherelike particles, like those formed via the PILP process,[17] were formed, suggesting the calcite substrate was indispensable to the formation of micropillars under the

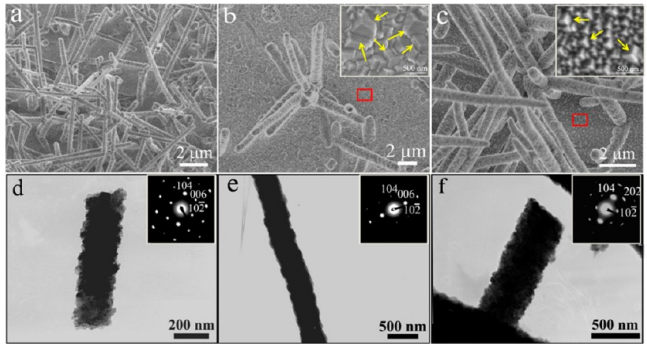

Figure 2. (a–c) SEM and (d–f) TEM images and (d–f inset) SAED patterns of calcite micropillars formed on various calcium carbonates substrates. (a, d) Polished calcite (001) substrates; (b, e) polished prismatic layers of mollusk shell; and (c, f) polished sea urchin tests. Concentrations of calcium chloride and PAA were 50 mM and 0.025 mg/mL, respectively. The crystallization proceeded at room temperature (27 °C) for 4 days. Red rectangles in b and c indicate the areas shown in insets of b and c, respectively.

dx.doi.org/10.1021/cg4010399 | Cryst. Growth Des. 2013, 13, 3856–3863

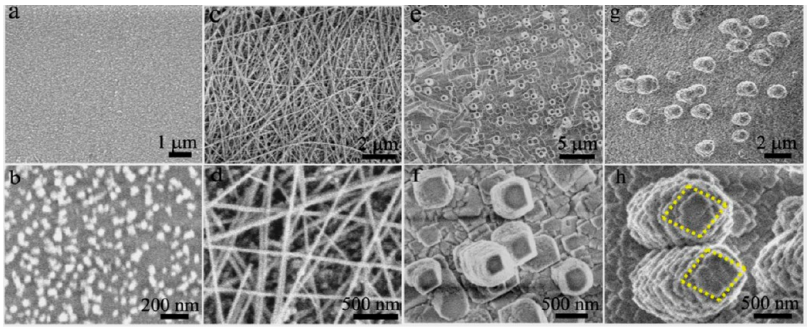

Figure 3. SEM images of calcite (104) substrates after different deposition times via diffusion method. (a, b) 1 day; (c, d) 2 days; and (e–h) 3 days. The concentration of calcium chloride and PAA were 50 mM and 0.025 mg/mL, respectively.

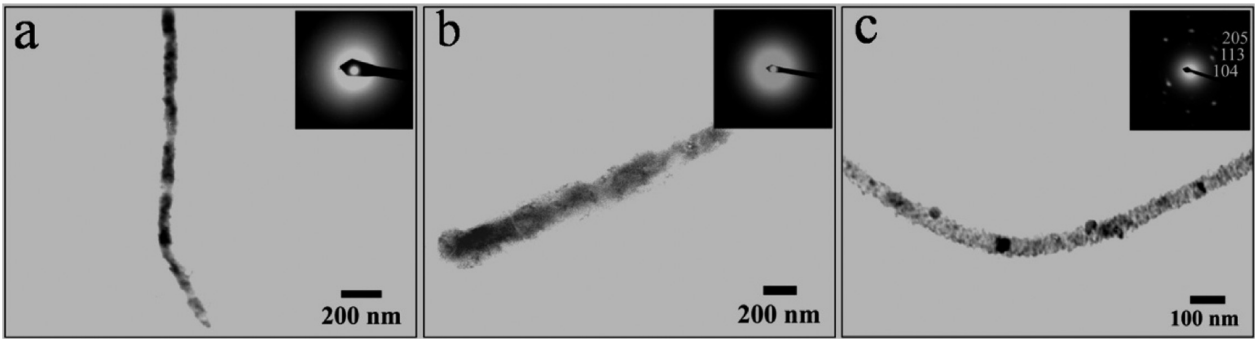

Figure 4. TEM images and ED patterns of various nanofibers. (a) Intermediate nanofibers formed after 2 days of reaction on calcite (104) substrates. (b) Nanofibers placed in 100% relative humidity for one day. (c) Nanofibers placed in an environment with both 100% RH and NH_4HCO_3 powder for one day.

current experimental conditions; this was consistent with the results of nanofibrous calcite formation on glass substrate only after the deposition of mineral, as reported by Meldrum[39,45] and Gower.[4,41]

3.1.3. Influence of PAA and Other Organic Molecules on the Formation of Calcite Micropillars. The influence of PAA concentrations on the formation of 1D calcite was studied. Only classical rhombohedral calcite plates appeared in the absence of PAA (Figure S9a of the Supporting Information), while short micropillars formed when 0.01 mg/mL of PAA was present in the reaction solution (Figure S9b of the Supporting Information). However, both the lengths and diameters of the 1D calcite decreased at higher PAA concentrations (0.05–0.1 mg/mL) (Figure S9, c and d, of theSupporting Information). As a rule of thumb, a higher concentration of PAA led to the formation of 1D calcium carbonate with reduced size, presumably due to the strong interaction between carboxylic groups of PAA and Ca^{2+}, resulting in suppression of crystal growth.[54] One possible explanation for this phenomenon is that the PAA–Ca complex nanofibers serve as a reservoir of Ca^{2+} for later formation of calcium carbonate. However, at a sufficiently high PAA concentration, the strong complexation of Ca^{2+} by PAA suppresses the release of Ca^{2+} and thus decreases the formation rate of calcite. So, it becomes more difficult to form calcite micropillars.

Other small organic molecules with the same concentrations were also used instead of PAA under similar reaction conditions. We found that rhombohedral calcite plates with the same orientation as the underlying substrates formed when L-glutamic acid (Figure S10a of the Supporting Information) and $NH_2(CH_2)_{10}Br$ (Figure S10b of the Supporting Information) were added in the mother solution, similar to those grown without any additives (Figure S9a of the Supporting Information). Other additives with low molecular weights also had little influence on the mineralization of calcium carbonate in our experiments. When aspartic acid alone was used, a large number of nanoparticles and microcrystals formed on calcite substrates (Figure S10c of the Supporting Information). Clearly, the results with PAA were unique. Our research group previously reported the formation of silver nanocolumns consisting of stacked nanoplates under the control of PAA,[55] forming a mesocrystalline structure similar to the 1D calcite micropillars of this work. Therefore, we conclude that the presence of PAA, which has many carboxylic groups that can coordinate with cations and has been shown to stabilize both PILP and amorphous precursors,[41] is a key ingredient for the formation of the calcite micropillars.

3.1.4. Growth Process of Calcite Micropillars. To investigate the formation mechanism, the growth of calcite micropillars on calcite (104) substrates was tracked by SEM (Figure 3) and AFM (Figure S11 of the Supporting Information). Only nanoparticles with sizes between 20 and 50 nm were seen on substrates after 1 day of reaction (Figure 3, panels a and b, and Figure S11b of the Supporting Information). In contrast, after 2 days of reaction, many long nanofibers with lengths of tens of micrometers could be observed over the entire surface of the calcite (104) substrates (Figure 3, panels c and d). AFM images (Figure S11c of the Supporting Information) further revealed that these nanofibers were composed of nanoparticles with similar shape and size to those of free nanoparticles around them. However, after crystallizing for 3 days, most of the long nanofibers disappeared and very short micropillars with flat rhombohedral (104) planes (Figure 3, panels e and f) or layered unsmooth microstructures

dx.doi.org/10.1021/cg4010399 | *Cryst. Growth Des.* 2013, 13, 3856–3863

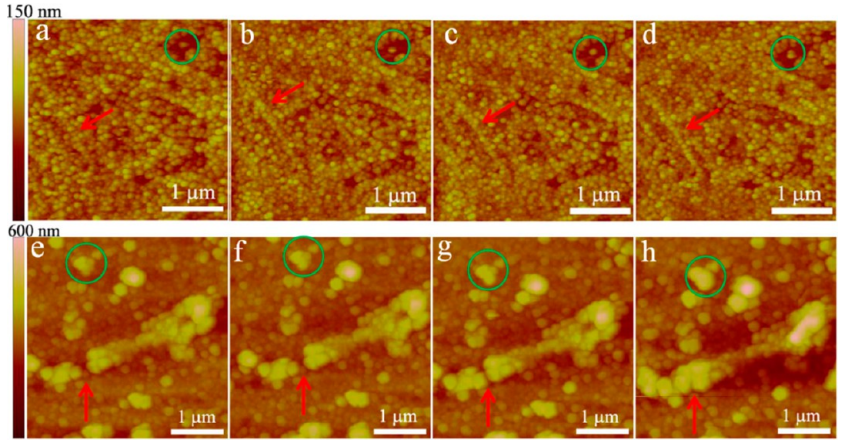

Figure 5. In situ AFM images of nanofibers formed on calcite (104) substrate by injecting a mixed solution of 15 mM calcium chloride, 0.025 mg/mL PAA, and 15 mM carbonate buffer into a fluid cell with a substrate. Reaction time: (a) 2 h, (b) 4 h, (c) 6 h, (d) 8 h, (e) 22 h, (f) 23 h, (g) 23.5 h, (h) 24 h. (a–d) and (e–h) were taken from two different regions on the same calcite (104) substrate. The circled particles provide reference points; red arrows indicate the positions of nanofibers.

appeared on the calcite (104) substrate (Figure 3, panels g and h, and Figure S11d of the Supporting Information). From side-view SEM images of micropillars, the lengths of those formed after three days of reaction were found to be less than 1 μm (Figure S12, panels a and b, of the Supporting Information), much shorter than those of micropillars formed after four days, most of which were around 10 μm (Figure S12, panels c and d, of the Supporting Information). Thus, the long nanofibers observed after two days of deposition time (Figure 3, panels c and d) were composed of a transient structure whose formation precedes that of the calcite micropillars.

3.2. Chemical Compositions of Nanofibers. Some long nanofibers were removed from the calcite substrate with a scalpel and were spread on TEM grids for further characterization. SAED patterns of these nanofibers lacked defined reflections, indicating that they were composed of an amorphous phase (Figure 4a). We hypothesized that the amorphous nanofibers were either ACC or a complex composed of PAA and Ca^{2+} (PAA-Ca). Experiments were designed to determine the chemical composition of the nanofibers. ACC will transform into calcite in the presence of pure water.[56] Thus, if the nanofibers were already ACC, the presence of CO_2 would not influence the transformation process. However, if they were a PAA–Ca complex then the presence of CO_2 in the presence of 100% humidity would contribute to the transformation to ACC and further crystallization to calcite.

When the nanofibers were kept in a chamber with 100% relative humidity (RH) for 1 day, they remained amorphous, as seen from the TEM image and the relative SAED pattern (Figure 4b). In contrast, in the presence of 100% RH and NH_4HCO_3 powder (provider for CO_2), the nanofibers transformed to well-crystallized calcite nanofibers, as indicated by the relative SAED patterns (Figure 4c). On the basis of these results, we conclude that the nanofibers were probably composed of the PAA–Ca complex or the PAA–Ca complex with inadequate carbonate.

3.3. In situ AFM Study on the Growth Process of Calcite Micropillars. To obtain real-time information on the formation process of the micropillars, in situ AFM was applied. However, the gas diffusion method was not suitable for in situ AFM studies because the fluid cell volume was not big enough to contain both a $CaCl_2$ solution and NH_4HCO_3 powder. Therefore, a mixing method was applied. While we were able to obtain 1D calcite structures and observe the development of some micropillars, by necessity, the concentrations of the reactants were very different from what were used in the bulk growth experiments. These concentrations were chosen through a process of trial and error in order to reproduce the results obtained in larger vessels by the gas diffusion method. However, there were still many differences between micropillars formed by these two distinct processes likely due to the differences in transport and reaction kinetics in the two distinct geometries.

Many nanoparticles about 70 nm in diameter appeared on the surface of the calcite substrates very soon after the injection of mixed solutions. The aggregation process of nanoparticles during the first 8 h was tracked, as shown in Figure 5, panels a–d. From the same field of view, one can see that, while some new nanoparticles appear with time, the dominant process is one of nanoparticle aggregation into 1D microstructures (red arrows), which become increasingly aligned along a straight line, as seen in Figure 5, panels a–d. The anisotropic alignment seems to be the result of aggregated nanoparticle movement, reorganization, and growth that might be directed by dipole–dipole effects or by the reduction of high surface energy by fusion of round calcium carbonate particles. After 20 h of mineralization, many large aggregates of nanoparticles with diameters of about 400 nm could be seen. Over time, the gap between two elongated aggregates of nanoparticles was filled by growth and coalescence of the initially deposited nanoparticles, combined with occasional deposition of new ones, so that a large microrod with a diameter of about 300 nm gradually formed (Figure 5, panels e–h). Moreover, microfacets appeared on the microrod, similar to that of short micropillars formed after 3 days of reaction via the gas diffusion method (Figure S11 of the Supporting Information). Surface reorganization and Ostwald ripening of aggregated nanoparticles are proposed as likely mechanisms for the formation of the microfacets.

We noted that these 1D microstructures, which formed in less than a day, were composed of nanoparticles having diameters of about 400 nm, which were considerably bigger than the diameters of the nanofibers (~50 nm) that were

dx.doi.org/10.1021/cg4010399 | Cryst. Growth Des. 2013, 13, 3856–3863

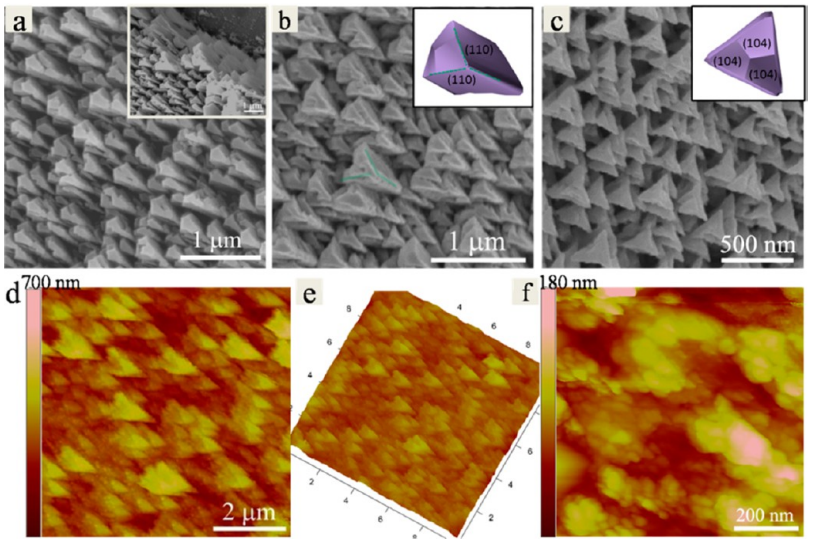

Figure 6. (a–c) SEM and (d–f) AFM images of polyhedral prism arrays formed on calcite (104) substrate by the mixing method. (a–c) SEM images of polyhedral prism arrays captured while tilting the sample holder for different angles. The angles between the electron beam and the calcite {104} plane (the surface of the calcite substrate) are (a, d, f) 90°, (b) 75°, and (c) 45°, respectively. (e) The corresponding 3D AFM image of the polyhedral prism array showed in (d). (f) A zoomed-in AFM image of the polyhedral prism array in (d). The concentrations of both calcium chloride and carbonate buffer were 10 mM, while the concentration of PAA was 0.01 mg/mL. The deposition time was 24 h.

composed of a PAA–Ca complex and which only formed after 2 days via the gas diffusion method. Thus, we assume that the 1D microstructures formed in Figure 5 are different from the PAA–Ca complex nanofibers in Figure 3 (panels c and d) and are instead composed of $CaCO_3$. Christenson et al.[57] reported that the size of reaction environment has a significant effect on the stabilities of ACC and mechanisms of mineral crystallization. The differences between in situ AFM studies and diffusion experiments in transport and reaction kinetics due to the small size of the reaction environment might be one of the primary reasons for the differences in the phase of the nanoparticles and the final morphologies of the samples.

The roughly spherical shape and consistent size suggests these constituent nanoparticles are not crystalline $CaCO_3$, while the lack of evidence for wetting of the calcite surface and the maintenance of distinct interparticle boundaries suggests that they are either solid or highly viscous at the time of attachment. None-the-less, the anisotropic alignment of the nanoparticles that comprise these structures (Figure 5), their eventual development into micropillars (Figure S11 of the Supporting Information) or oriented polygon particles (see below and Figure S13 of the Supporting Information), combined with their contact to (104) calcite faces implies an attachment bias typically associated with crystalline particles.[27]

Thus, we propose that these 1D structures formed through a self-organization process that started with deposition of PAA-stabilized nanoparticles, likely comprised of ACC or partially solidified PILP, onto the underlying calcite substrate. The latter acted as a template to direct crystallization of the nanoparticles with the same orientation. Further attachment of nanoparticles was biased along certain directions, though the source and nature of the force leading to that bias remains unknown. Whether this same process is responsible for the roughening of the underlying substrate seen in Figure 1 cannot be stated with certainty. However, the general coverage of the surface by nanoparticles at early times, before micropillars begin to emerge, suggests it is, though true epitaxial growth through step propagation cannot be ruled out.

3.4. Characterizations of Calcite Polyhedral Prism Arrays. *3.4.1. SEM Studies on Polyhedral Prism Arrays.* When concentrations of $CaCl_2$ and PAA in the mother solutions were decreased from 50 mM and 0.025 mg/mL to 10 mM and 0.01 mg/mL, respectively, the mixing method produced coaligned prism arrays after 1 day of deposition on calcite (104) substrates, as seen in Figure 6 (panels a–c), which presents SEM images collected at different angles. Arrays of polyhedra were observed when the electron beam was perpendicular to the calcite {104} plane [i.e., the surface of the calcite substrate (Figure 6a)]. When the sample holder was tilted until the electron beam was incident at 75° to the calcite {104} plane, prisms with one relatively smooth top face and two coarse side faces were seen (Figure 6b). Figure 6c shows ordered quasi-triangular microstructure arrays after tilting the electron beam to be incident at 45° to the calcite {104} plane. Given that the interfacial angle between the {104} and (001) planes of calcite is 44.6°, the SEM image in Figure 6c was taken while the electron beam was only 0.4° off of the [001] axis of calcite. Considering together the SEM images taken from different directions in Figure 6 (panels a–c), we propose that these polyhedral prisms, like the pillars, extend from the (104) calcite substrate along the [001] axis and are capped by three (104) facets, as shown by the insets to Figure 5 (panels b and c). Whether the side faces of the polyhedral prisms are true crystallographic faces or simply pseudo-(110) faces is unclear. This geometry is consistent with the facets expressed on the micropillars formed under higher concentrations of $CaCl_2$ and PAA in the mother solutions via the gas diffusion method (Figure 1). Moreover, from AFM images (Figure 6, panels d–f), it is clear that these polyhedral were actually composed of nanoparticles, further presenting the similarities between calcite micropillar and polyhedron. Similar polyhedral arrays were reported by Sethmann et al., who concluded that they grew from a gelatinous film that first formed on the calcite surface before morphing into a microfaceted morphology.[58] In this work, we show that polyhedral arrays could also form through deposition and reorganization of nanoparticles.

dx.doi.org/10.1021/cg4010399 | *Cryst. Growth Des.* 2013, 13, 3856–3863

3.4.2. In situ AFM Study on the Formation Process of Polyhedral Prisms. In order to understand the formation process of these polyhedral microstructures, in situ AFM was applied. The AFM images show that, during the first hour, many etch pits formed on (104) calcite substrate (Figure S13, panels a–d, of the Supporting Information), indicating that dissolution of the calcite surface occurred initially. We note that the mixed solution became cloudy after sodium bicarbonate aqueous solution was added into the solution with $CaCl_2$ and PAA and turned clear again after 1 h. The chemical composition of the cloudy solution was characterized using an infrared spectrometer (Figure S14 of the Supporting Information). The strong peak at about 3140 and 1680 cm^{-1} can be attributed to the characteristic bands of carboxyl groups in PAA. Compared with that of PAA, the peak intensity of the C=O stretching vibration band at 1680 cm^{-1} was diminished, and the peak position was shifted to lower wavenumbers in the spectra of both PAA–Ca solids collected from nanofibers and these cloudy solutions, probably due to the strong electrostatic interactions between the carboxylic groups in PAA and Ca^{2+}. This is consistent with previously reported results.[43] Thus, we propose that calcium ions first coordinated with PAA, thereby decreasing the calcium ion activity in the $CaCl_2$ plus PAA solution. This resulted in an undersaturated solution with respect to calcite and, hence, the dissolution of the calcite substrate. However, the PAA–Ca complex was not stable in sodium bicarbonate aqueous solutions and thus the more stable calcium carbonate nanoparticles eventually formed.

After 4 h, many nanoparticles were observed on the surface of the calcite substrate (Figure S13e of the Supporting Information). Within about 7.5 h, the deposition, reorganization, growth, and coalescence of nanoparticles from the solution resulted in gradual development of large, coaligned polyhedral aggregates with a triangular shape (Figure S13, panels f–h, of the Supporting Information) similar to those seen in the SEM images described above. Though the final stage of the polyhedral particles was not observed by in situ AFM, the formation of these structures through aggregation and growth of nanoparticles was clear and convincing. Thus, $CaCO_3$ mesocrystals of distinct morphologies, 1D microstructures and 3D prisms, were achieved in two similar conditions through the same mechanism of nanoparticle assembly. These findings indicate that formation of hierarchical calcium carbonate microstructures on calcite substrates in the presence of PAA in our experiments occurs through a process of anisotropic nanoparticle aggregation and fusion, accompanied by growth and surface reorganization or Ostwald ripening.

4. CONCLUSIONS

Our work demonstrates the successful synthesis from PAA-bearing solution of well-aligned calcite micropillars. Both the substrate and the soluble organic PAA are indispensable to the formation of these micropillars. We hypothesize that PAA temporarily stabilizes liquidlike or amorphous precursor particles, while the calcite substrate is used to control crystal orientation of the crystallizing particles, which in turn act as the building blocks of these 1D structures. The appearance of these structures is preceded by the formation and disappearance of nanofibers, which FT-IR and TEM studies show are comprised of a PAA–Ca intermediate phase. These structures are reminiscent of calcium carbonate fibers made from a Ca-polymer precursor.[43] Time dependent observations under conditions adjusted to obtain similar structures in the small-volume fluid cell of an AFM show that micropillar formation in these conditions is preceded by formation of transient nanoparticles. Moreover, our results show that, with slightly less PAA, the same basic process leads to formation of 3D polyhedral prisms with triangular cross sections in both bulk and AFM experiments.

The AFM results imply that anisotropic nanoparticle aggregation, which is the hallmark of the mesocrystal growth mechanism,[59−61] is essential for the formation of both the 1D and the 3D structures under similar experimental conditions, though growth of the nanoparticles along with reorganization and ripening are key processes. The results may have implications for the formation of both 1D and 3D biogenic minerals that form in organisms with both soluble molecules, such as polysaccharides, peptides, and proteins, and insoluble matrices. For some of these mineral structures, like that of the sea urchin spicule, their development from an aggregate of amorphous nanoparticles that crystallize with an orientation determined by a single crystal template is well-documented.[62,63] In conclusion, though the basic characteristics of $CaCO_3$ mesocrystals are already well-described,[24] this work provides real time observations of the nanoparticle aggregation process, which may provide new insights into biomineralization mechanisms.

■ ASSOCIATED CONTENT

Ⓢ Supporting Information

SEM characterization of substrates before use, detailed information of micropillars, including the polarized optical microscope images, TEM and corresponding ED patterns, FT-IR spectra and AFM images, influences of different additives, the concentration of additive, silica, and glass substrates, and in situ AFM images of the formation process of polygon prism. This material is available free of charge via the Internet at http://pubs.acs.org.

■ AUTHOR INFORMATION

Corresponding Author

*Y.M.: e-mail, yurong.ma@pku.edu.cn; L.Q.: e-mail, liminqi@pku.edu.cn; J.J.Y.: e-mail, jjdeyoreo@lbl.gov.

Funding

Notes

The authors declare no competing financial interest.

■ ACKNOWLEDGMENTS

Financial support from the National Natural Science Foundation of China (Grants 51272298, 21173010, 21073005, and 51121091), China Scholarship Council are gratefully acknowledged. The AFM studies were supported by the Division of Chemical Sciences, Geosciences, and Biosciences of the US Department of Energy and performed at the Molecular Foundry, Lawrence Berkeley National Laboratory, an Office of Science, Office of Basic Energy Sciences, Scientific User Facility under Contract DE-AC02-05CH11231.

■ REFERENCES

(1) Cölfen, H. *Curr. Opin. Colloid Interface Sci.* **2003**, *8*, 23.
(2) Meldrum, F. C.; Cölfen, H. *Chem. Rev.* **2008**, *108*, 4332.
(3) Cusack, M.; Freer, A. *Chem. Rev.* **2008**, *108*, 4433.
(4) Gower, L. B. *Chem. Rev.* **2008**, *108*, 4551.

(5) Aizenberg, J.; Tkachenko, A.; Weiner, S.; Addadi, L.; Hendler, G. *Nature* **2001**, *412*, 819.
(6) Sommerdijk, N.; De With, G. *Chem. Rev.* **2008**, *108*, 4499.
(7) Politi, Y.; Arad, T.; Klein, E.; Weiner, S.; Addadi, L. *Science* **2004**, *306*, 1161.
(8) Feng, Q. L.; Li, H. B.; Pu, G.; Zhang, D. M.; Cui, F. Z.; Li, H. D.; Kim, T. N. *J. Mater. Sci.* **2000**, *35*, 3337.
(9) Berman, A.; Hanson, J.; Leiserowitz, L.; Koetzle, T. F.; Weiner, S.; Addadi, L. *Science* **1993**, *259*, 776.
(10) Ma, Y. R.; Aichmayer, B.; Paris, O.; Fratzl, P.; Meibom, A.; Metzler, R. A.; Politi, Y.; Addadi, L.; Gilbert, P.; Weiner, S. *Proc. Natl. Acad. Sci. U.S.A.* **2009**, *106*, 6048.
(11) Mann, S. *Biomineralization, Principles and Concepts in Bioinorganic Materials Chemistry*; Oxford University Press: Oxford, 2001.
(12) Addadi, L.; Raz, S.; Weiner, S. *Adv. Mater.* **2003**, *15*, 959.
(13) Loste, E.; Park, R. J.; Warren, J.; Meldrum, F. C. *Adv. Funct. Mater.* **2004**, *14*, 1211.
(14) Gonga, Y. U. T.; Killiana, C. E.; Olson, I. C.; Appathurai, N. P.; Amasino, A. L.; Martin, M. C.; Holt, L. J.; Wilt, F. H.; Gilbert, P. U. P. A. *Proc. Natl. Acad. Sci. U.S.A.* **2012**, *109*, 6088.
(15) Stanley, S. M.; Ries, J. B.; Hardie, L. A. *Proc. Natl. Acad. Sci. U.S.A.* **2002**, *99*, 15323.
(16) Gal, A.; Weiner, S.; Addadi, L. *J. Am. Chem. Soc.* **2010**, *132*, 13208.
(17) Gower, L. B.; Odom, D. J. *J. Cryst. Growth* **2000**, *210*, 719.
(18) Gower, L. A.; Tirrell, D. A. *J. Cryst. Growth* **1998**, *191*, 153.
(19) Dai, L. J.; Douglas, E. P.; Gower, L. B. *J. Non-Cryst. Solids* **2008**, *354*, 1845.
(20) Kellermeier, M.; Gebauer, D.; Melero-Garcia, E.; Drechsler, M.; Talmon, Y.; Kienle, L.; Cölfen, H.; Garcia-Ruiz, J. M.; W., K. *Adv. Funct. Mater.* **2012**, *22*, 4301.
(21) Kellermeier, M.; Melero-Garcia, E.; Glaab, F.; Klein, R.; Drechsler, M.; Rachel, R.; Garcia-Ruiz, J. M.; Kunz, W. *J. Am. Chem. Soc.* **2010**, *132*, 17859.
(22) Bassett, D. C.; Marelli, B.; Nazhat, S. N.; Barralet, J. E. *Adv. Funct. Mater.* **2012**, *22*, 3460.
(23) Gebauer, D.; Völkel, A.; Cölfen, H. *Science* **2008**, *322*, 1819.
(24) Song, R. Q.; Cölfen, H. *Adv. Mater.* **2010**, *22*, 1301.
(25) Song, R. Q.; Cölfen, H. *CrystEngComm* **2011**, *13*, 1249.
(26) Cölfen, H.; Antonietti, M. *Mesocrystals and Nonclassical Crystallization*; Wiley: New York, 2008.
(27) Li, D.; Nielsen, M. H.; Lee, J. R.; Frandsen, C.; Banfield, J.; De Yoreo, J. J. *Science* **2012**, *366*, 1014.
(28) Yang, D.; Qi, L. M.; Ma, J. M. *Chem. Commun.* **2003**, 1180.
(29) Kulak, A. N.; Iddon, P.; Li, Y. T.; Armes, S. P.; Cölfen, H.; Paris, O.; Wilson, R. M.; Meldrum, F. C. *J. Am. Chem. Soc.* **2007**, *129*, 3729.
(30) Mukkamala, S. B.; Powell, A. K. *Chem. Commun.* **2004**, 918.
(31) Aizenberg, J.; Muller, D. A.; Grazul, J. L.; Hamann, D. R. *Science* **2003**, *299*, 1205.
(32) Li, C.; Qi, L. M. *Angew. Chem., Int. Ed.* **2008**, *47*, 2388.
(33) Weiner, S.; Addadi, L.; Wagner, H. D. *Mater. Sci. Eng., C* **2000**, *11*, 1.
(34) Li, H. Y.; Xin, H. L.; Muller, D. A.; Estroff, L. A. *Science* **2009**, *326*, 1244.
(35) Long, X.; Ma, Y. R.; Qi, L. M. *Cryst. Growth Des.* **2011**, *11*, 2866.
(36) Kim, Y. Y.; Ganesan, K.; Yang, P. C.; Kulak, A. N.; Borukhin, S.; Pechook, S.; Ribeiro, L.; Kröger, R.; Eichhorn, S. J.; Armes, S. P.; Pokroy, B.; Meldrum, F. C. *Nat. Mater.* **2011**, *10*, 890.
(37) Loste, E.; Meldrum, F. C. *Chem. Commun.* **2001**, 901.
(38) Zhu, J. H.; Song, J. M.; Yu, S. H.; Zhang, W. Q.; Shi, J. X. *CrystEngComm* **2009**, *11*, 539.
(39) Kim, Y. Y.; Kulak, A. N.; Li, Y. T.; Batten, T.; Kuball, M.; Armes, S. P.; Meldrum, F. C. *J. Mater. Chem.* **2009**, *19*, 387.
(40) Olszta, M. J.; Odom, D. J.; Douglas, E. P.; Gower, L. B. *Connect. Tissue Res.* **2003**, *44*, 326.
(41) Olszta, M. J.; Gajjeraman, S.; Kaufman, M.; Gower, L. B. *Chem. Mater.* **2004**, *16*, 2355.
(42) Balz, M.; Therese, H. A.; Li, J. X.; Gutmann, J. S.; Kappl, M.; Nasdala, L.; Hofmeister, W.; Butt, H. J.; Tremel, W. *Adv. Funct. Mater.* **2005**, *15*, 683.
(43) You, C.; Zhang, Q. A.; Zhao, Y.; Jiao, Q. Z. *Cryst. Res. Technol.* **2011**, *46*, 69.
(44) Miura, T.; Kotachi, A.; Oaki, Y.; Imai, H. *Cryst. Growth Des.* **2006**, *6*, 612.
(45) Cantaert, B.; Kim, Y. Y.; Ludwig, H.; Nudelman, F.; Sommerdijk, N. A. J. M.; Meldrum, F. C. *Adv. Funct. Mater.* **2012**, *22*, 907.
(46) Viravaidya, C.; Li, M.; Mann, S. *Chem. Commun.* **2004**, 2181.
(47) Liu, D. X.; Yates, M. Z. *Langmuir* **2006**, *22*, 5566.
(48) Burazerovic, S.; Gradinaru, J.; Pierron, J.; Ward, T. R. *Angew. Chem., Int. Ed.* **2007**, *46*, 5510.
(49) Homeijer, S. J.; Barrett, R. A.; Gower, L. B. *Cryst. Growth Des.* **2010**, *10*, 1040.
(50) Chung, S. W.; Shina, S. H.; B., C. R.; De Yoreo, J. J. *Proc. Natl. Acad. Sci. U.S.A.* **2010**, *107*, 16536.
(51) Davis, K. J.; Dove, P. M.; De Yoreo, J. J. *Science* **2000**, *290*, 1134.
(52) Stephenson, A. E.; De Yoreo, J. J.; Wu, L.; Wu, K. J.; Hoyer, J.; Dove, P. M. *Science* **2008**, *322*, 724.
(53) Olszta, M. J.; Gajjeraman, S.; Kaufman, M.; Gower, L. B. *Chem. Mater.* **2004**, *16*, 2355.
(54) Yu, J. G.; Lei, M.; Cheng, B.; Zhao, X. J. *J. Solid State Chem.* **2004**, *177*, 681.
(55) Bai, J. W.; Qin, Y.; Jiang, C. Y.; Qi, L. M. *Chem. Mater.* **2007**, *19*, 3367.
(56) Ma, Y. R.; Weiner, S.; Addadi, L. *Adv. Funct. Mater.* **2007**, *17*, 2693.
(57) Stephens, C. J.; Ladden, S. F.; Meldrum, F. C.; Christenson, H. K. *Adv. Funct. Mater.* **2010**, *20*, 2108.
(58) Sethman, I.; Putnis, A.; Grassmann, O.; Lobmann, P. *Am. Mineral.* **2005**, *90*, 1213.
(59) Lee Penn, R.; Jillian, F. B. *Am. Mineral.* **1998**, *83*, 1077.
(60) Lee Penn, R.; Jillian, F. B. *Science* **1998**, *281*, 969.
(61) Gilbert, B.; Zhang, H.; Huang, F.; Finnegan, M. P.; Waychunas, G. A.; Banfield, J. F. *Geochim. Cosmochim. Acta* **1999**, *63*, 1549.
(62) Beniash, E.; Aizenberg, J.; Addadi, L.; Weiner, S. *Proc. R. Soc. London, Ser. B* **1997**, *264*, 461.
(63) Politi, Y.; Metzler, R. A.; Abrecht, M.; Gilbert, B.; Wilt, F.; Sagi, I.; Addadi, L.; Weiner, S.; Gilbert, P. U. P. A. *Proc. Natl. Acad. Sci. U.S.A.* **2008**, *105*, 17362.